Computational Mechanics 34 (2004) 137–146 © Springer-Verlag 2004
DOI 10.1007/s00466-004-0561-5

Modified smoothed particle hydrodynamics method and its application to transient problems

G. M. Zhang, R. C. Batra

Abstract A modification to the smoothed particle hydrodynamics method is proposed that improves the accuracy of the approximation especially at points near the boundary of the domain. The modified method is used to study one-dimensional wave propagation and two-dimensional transient heat conduction problems.

Keywords Meshless method, One-dimensional elastodynamics, Two-dimensional transient heat conduction

1 Introduction

The smoothed particle hydrodynamics (SPH) method is one of the earliest mesh free methods employing Lagrangian description of motion. It was proposed by Lucy (1977) and Gingold and Monaghan (1977) to analyze astrophysical problems in a three-dimensional space. Libersky and Petschek (1990) extended it to study the dynamic response of materials. The method has been applied to several classes of problems, such as free surface flows (Monaghan 1994), explosion phenomenon (Liu et al. 2003), impact and penetration (Randles et al. 1995, Johnson et al. 1996); see Chen et al. (1999) for additional references. The performance of the method has been extended by using parallel computing techniques (Medina and Chen 2000).

As is well known, the SPH method is not even zero-order consistent near the boundary. Liu et al. (1995a, b) improved its consistency by introducing a corrective kernel which is a product of the correction function and the original kernel; the improved method is called the reproducing kernel particle method (RKPM). The correction is a polynomial in the spatial coordinates and the RKPM can be nth-order consistent. Chen et al. (1999a, b) proposed a corrective smoothed-particle method (CSPM) to address the tensile instability and the inconsistency problems in the conventional SPH method. Here we propose a modification to the CSPM that improves its accuracy especially at points near the boundary of the domain.

The paper is organized as follows. Section 2 discusses the conventional SPH method. The modified SPH (MSPH) method is given in Sect. 3 where numerical tests to show its superiority over the CSPM are reviewed. In Sect. 4, the MSPH method is applied to study wave propagation in an elastic bar, and 2-dimensional transient heat conduction in a plate. Section 5 summarizes conclusions.

2 Conventional SPH method

In the SPH method, the approximate value $\tilde{f}(\mathbf{x})$ of a function f at a point $\mathbf{x}$ in domain Ω is given by

$$\tilde{f}(\mathbf{x}) = \int_{\Omega} f(\xi) W(\mathbf{x} - \xi, h) \mathrm{d}\xi \quad , \tag{2.1}$$

where $W(\mathbf{x} - \xi)$ is a kernel or a smoothing function. The approximate value $\tilde{f}$ of f depends upon two parameters; the kernel W and the dilation h which determines the support of W. The kernel function, W, is required to have the following properties:

(i) $W(\mathbf{x} - \xi, h) = 0$ for $|\mathbf{x} - \xi| \geq 2h$,
(ii) $\int_{\Omega} W(\mathbf{x} - \xi, h) d\xi = 1$,
(iii) $\lim_{h\to 0} W(\mathbf{x} - \xi, h) = \delta(\mathbf{x} - \xi)$ where δ is the Dirac delta function,
(iv) $W(\mathbf{x} - \xi, h) \geq 0$,
(v) $W(\mathbf{x} - \xi, h) = W(\xi - \mathbf{x}, h)$.

The spatial derivative, ∇f, at the point $\mathbf{x}$ is approximated by

$$\begin{aligned}\nabla\tilde{f}(\mathbf{x}) &= \int_{\Omega} \nabla f(\xi) W(\mathbf{x} - \xi, h) \mathrm{d}\xi \\ &= -\int_{\Omega} f(\xi) \nabla W(\mathbf{x} - \xi, h) \mathrm{d}\xi \quad ,\end{aligned} \tag{2.2}$$

where we have integrated by parts and used property (i) of the kernel function W.

Received: 22 September 2003/Accepted: 11 February 2004
Published online: 23 March 2004

G. M. Zhang, R. C. Batra (✉)
Department of Engineering Science and Mechanics,
MC 0219 Virginia Polytechnic Institute and State
University Blacksburg, VA 24061, USA
E-mail: rbatra@vt.edu

This work was supported by the ONR grant N00014-98-1-0300 and the ARO grant DAAD19-01-1-0657 to Virginia Polytechnic Institute and State University, and the AFOSR MURI grant to Georgia Tech that awarded a subcontract to Virginia Polytechnic Institute and State University. Opinions expressed in the paper are those of authors and not of the funding agencies.

For numerical work the integral (2.1) is approximated by imagining that the mass in Ω is divided into N particles of masses $m_1, m_2, \ldots, m_N$ and densities $\rho_1, \rho_2, \ldots, \rho_N$ respectively. The value f_i of the integral (2.1) for the ith particle is approximated by

$$f_i = \sum_{j=1}^{N} m_j f_j W_{ij}/\rho_j; \quad W_{ij} = W(\mathbf{x}^{(i)} - \boldsymbol{\xi}^{(j)}) \ . \tag{2.3}$$

Because of the compact support of the kernel function W, the number of particles used in the summation (2.3) is smaller than N. Similarly, Eq. (2.2) is approximated by

$$\begin{aligned} f_{\alpha i} &\equiv \frac{\partial f}{\partial x_\alpha^{(i)}} = -\sum_{j=1}^{N} m_j f_j W_{ij,\alpha}/\rho_j, \\ W_{ij,\alpha} &= -\left.\frac{\partial W}{\partial x_\alpha}\right|_{\mathbf{x}=\mathbf{x}^{(i)}, \xi=\xi^{(j)}}, \quad \alpha = 1,2,3 \ . \end{aligned} \tag{2.4}$$

The range of index α equals the spatial dimension of the domain Ω. For a constant function $f(\mathbf{x}) = f_i$ Eq. (2.4) gives

$$\sum_{j=1}^{N} m_j f_i W_{ij,\alpha}/\rho_j = 0 \ . \tag{2.5}$$

Addition of (2.5) and $(2.4)_1$ gives

$$f_{\alpha i} = -\sum_{j=1}^{N} m_j (f_j - f_i) W_{ij,\alpha}/\rho_j \ . \tag{2.6}$$

One can similarly deduce the following approximation for the second-order derivatives:

$$f_{\alpha\beta i} = \sum_{j=1}^{N} m_j (f_j - f_i) W_{ij,\alpha\beta}/\rho_j \ , \tag{2.7}$$

where

$$\begin{aligned} f_{\alpha\beta i} &= \left.\frac{\partial^2 f}{\partial x_\alpha \partial x_\beta}\right|_{\mathbf{x}=\mathbf{x}^{(i)}}, \\ W_{ij,\alpha\beta} &= \left.\frac{\partial^2 W}{\partial x_\alpha \partial x_\beta}\right|_{\mathbf{x}=\mathbf{x}^{(i)}, \xi=\xi^{(j)}} \ . \end{aligned} \tag{2.8}$$

3 Modified SPH (MSPH) method

3.1 Discretization

Using Taylor series expansion of $f(\mathbf{x})$ about the point $\mathbf{x} = \mathbf{x}^{(i)}$ and retaining only three terms in the series, we obtain

$$\begin{aligned} f(\boldsymbol{\xi}) \simeq\ & f(\mathbf{x}^{(i)}) + \frac{\partial f}{\partial x_\alpha^{(i)}}(\xi_\alpha - x_\alpha^{(i)}) \\ & + \frac{1}{2}\frac{\partial^2 f}{\partial x_\alpha^{(i)} \partial x_\beta^{(i)}}(\xi_\alpha - x_\alpha^{(i)})(\xi_\beta - x_\beta^{(i)}) \ , \end{aligned} \tag{3.1}$$

where summation is implied on repeated indices α and β. Multiplication of both sides of (3.1) with the kernel function $W(\mathbf{x} - \boldsymbol{\xi}, h)$ and integration of the resulting equation over the domain Ω yield

$$\begin{aligned} \int_\Omega f(\boldsymbol{\xi}) W \mathrm{d}\boldsymbol{\xi} =\ & f_i \int_\Omega W \mathrm{d}\boldsymbol{\xi} + f_{\alpha i} \int_\Omega (\xi_\alpha - x_\alpha^{(i)}) W \mathrm{d}\boldsymbol{\xi} \\ & + \frac{1}{2} f_{\alpha\beta i} \int_\Omega (\xi_\alpha - x_\alpha^{(i)})(\xi_\beta - x_\beta^{(i)}) W \mathrm{d}\boldsymbol{\xi} \ . \end{aligned} \tag{3.2}$$

Repeating the above procedure with W replaced by $W_\gamma = \partial W/\partial \xi_\gamma$ and $W_{\gamma\delta} = \partial^2 W/\partial \xi_\gamma \partial \xi_\delta$, we obtain

$$\begin{aligned} \int_\Omega f(\boldsymbol{\xi}) W_\gamma \mathrm{d}\boldsymbol{\xi} =\ & f_i \int_\Omega W_\gamma \mathrm{d}\boldsymbol{\xi} + f_{\alpha i} \int_\Omega (\xi_\alpha - x_\alpha^{(i)}) W_\gamma \mathrm{d}\boldsymbol{\xi} \\ & + \frac{1}{2} f_{\alpha\beta i} \int_\Omega (\xi_\alpha - x_\alpha^{(i)})(\xi_\beta - x_\beta^{(i)}) W_\gamma \mathrm{d}\boldsymbol{\xi} \ , \end{aligned} \tag{3.3}$$

$$\begin{aligned} \int_\Omega f(\boldsymbol{\xi}) W_{\gamma\delta} \mathrm{d}\boldsymbol{\xi} =\ & f_i \int_\Omega W_{\gamma\delta} \mathrm{d}\boldsymbol{\xi} + f_{\alpha i} \int_\Omega (\xi_\alpha - x_\alpha^{(i)}) W_{\gamma\delta} \mathrm{d}\boldsymbol{\xi} \\ & + \frac{1}{2} f_{\alpha\beta i} \int_\Omega (\xi_\alpha - x_\alpha^{(i)})\ (\xi_\beta - x_\beta^{(i)}) W_{\gamma\delta} \mathrm{d}\boldsymbol{\xi} \ . \end{aligned} \tag{3.4}$$

Equations (3.2), (3.3) and (3.4) for $\alpha, \beta = 1,2,3$ constitute ten equations for the ten unknowns f_i, $f_{\alpha i}$ and $f_{\alpha\beta i}$ at the point $\mathbf{x} = \mathbf{x}^{(i)}$. We write these equations as

$$\mathbf{T} = \mathbf{BF} \text{ or } B_{IJ} F_J = T_I, \quad I = 1,2,\ldots,10 \ , \tag{3.5}$$

where

$$B_{IJ} = \int_\Omega \Phi(I)\Theta(J) \mathrm{d}\boldsymbol{\xi} = \sum_{j=1}^{N} \Phi(I)\Theta(J) m_j/\rho_j \ ; \tag{3.6}$$

$$\begin{aligned} &\Phi(1) = W_{ij},\ \Phi(2) = W_{ij,x},\ \Phi(3) = W_{ij,y}, \Phi(4) = W_{ij,z} \ , \\ &\Phi(5) = W_{ij,xx},\ \Phi(6) = W_{ij,yy},\ \Phi(7) = W_{ij,zz} \ , \\ &\Phi(8) = W_{ij,xy},\ \Phi(9) = W_{ij,yz},\ \Phi(10) = W_{ij,xz} \ ; \end{aligned} \tag{3.7}$$

$$\begin{aligned} &\Theta(1) = 1,\ \Theta(2) = x_j - x_i,\ \Theta(3) = y_j - y_i \ , \\ &\Theta(4) = z_j - z_i,\ \Theta(5) = \frac{1}{2}(x_j - x_i)^2 \ , \\ &\Theta(6) = \frac{1}{2}(y_j - y_i)^2,\ \Theta(7) = \frac{1}{2}(z_j - z_i)^2 \ , \\ &\Theta(8) = (x_j - x_i)(y_j - y_i),\ \Theta(9) = (y_j - y_i)(z_j - z_i) \ , \\ &\Theta(10) = (x_j - x_i)(z_j - z_i) \ ; \end{aligned} \tag{3.8}$$

$$\begin{aligned} &F = \{f_i, f_{xi}, f_{yi}, f_{zi}, f_{xxi}, f_{yyi}, f_{zzi}, f_{xyi}, f_{yzi}, f_{zxi}\}^T \ , \\ &T_I = \sum_{j=1}^{N} f_j \Phi(I) m_j/\rho_j \ . \end{aligned} \tag{3.9}$$

Equation (3.5) is solved for $F_1, F_2, \ldots, F_{10}$ and the result is substituted in equation (3.1). Retention of third-order derivatives in the expansion (3.1) will result in a system of

20 simultaneous equations like (3.5). With (3.1), the error in the value of $f(\xi)$ is of the order $|\xi - \mathbf{x}^{(i)}|^3$.

In order for the matrix $\mathbf{B}$ defined by (3.6) to be nonsingular, N must be at least 3, 6 and 10 for one-, two- and three-dimensional problems respectively.

3.2
Consistency

For the MSPH method proposed in Sect. 3.1, the kernel estimate of a function is clearly mth order consistent if $(m+1)$ terms are retained in the Taylor series expansion (3.1) since the function and its first m derivatives are exactly reproduced by the approximation scheme. However, the kernel estimates of the first- and the second-order derivatives have consistencies of orders $(m-1)$ and $(m-2)$ respectively. The number of simultaneous algebraic equations (3.5) to be solved increases rapidly with an increase in the value of m.

3.3
Comparison with the corrective SPH method

If the first-order and the second-order derivative terms in Eq. (3.1) are neglected, then the kernel estimate of $f(\mathbf{x})$ is given by

$$f_i = \int_\Omega f(\xi) W(\mathbf{x}^{(i)} - \xi) \mathrm{d}\xi \Big/ \int_\Omega W(\mathbf{x}^{(i)} - \xi) \mathrm{d}\xi \ , \qquad (3.10)$$

or in particle summation form by

$$f_i = \sum_{j=1}^{N} (f_j W_{ij} m_j/\rho_j) \Big/ \sum_{j=1}^{N} (W_{ij} m_j/\rho_j) \ . \qquad (3.11)$$

Because of the property (v) of the kernel, $\int_\Omega (\mathbf{x} - \xi) W(\mathbf{x} - \xi) \mathrm{d}\xi = 0$. Thus the error in (3.10) is of the order $|\mathbf{x} - \mathbf{x}^{(i)}|^2$ for interior particles, and of order $|\mathbf{x} - \mathbf{x}^{(i)}|$ for particles on or near the boundaries. The property (ii) of the kernel implies that for particles away from the boundaries, Eqs. (3.10) and (3.11) reduce to (2.1) and (2.3) respectively. However, for particles near the boundary, Eq. (3.11) gives better results than those obtained from (2.3).

The present method differs from the CSPM of Chen et al. (1999a, b) in the following two respects. Chen et al. (1999a, b) solve the system of Eq. (3.5) by splitting it into three sets of equations: $T_1 = B_{11}F_1$; $T_I = B_{IJ}F_J$, $I,J = 2,3,4$; $T_I = B_{IJ}F_J$; $I,J = 5,6,\ldots,10$. However, we solve (3.5) simultaneously for the ten variables $F_1, F_2, \ldots, F_{10}$. Since values of F_2, F_3, F_4 depend upon that of F_1, and of F_5 through F_{10} upon the values of F_1, F_2, F_3 and F_4, an error in finding F_1 through F_4 at particles near the boundary will adversely affect values of F_5 through F_{10}. Whereas we use the kernel estimate value of f_i in Eq. (3.5), in the CSPM f_i equals the value of f at the particle i. The CSPM requires less CPU time than the present method since it solves three smaller sets of equations than the present method in which ten equations are solved simultaneously for the ten unknowns.

In the following discussion, we designate the present method as the modified SPH (MSPH) method. The kernel is taken to be the Gauss function, i.e.,

$$W(\mathbf{x} - \xi) = \begin{cases} \frac{A}{(h\sqrt{\pi})^n} \left(e^{-(|\mathbf{x}-\xi|^2/h^2)} - e^{-4} \right), & |\mathbf{x} - \xi| \le 2h \ , \\ 0, & |\mathbf{x} - \xi| \ge 2h \ , \end{cases} \qquad (3.12)$$

where n equals the dimensionality of the space, and the normalization parameter A equals 1.04823, 1.10081 and 1.18516 for $n = 1, 2$ and 3 respectively.

3.4
Numerical tests

3.4.1
One-dimensional domain

Consider the function

$$f(x) = (x - 0.5)^4, \quad x \in [0, 1] \ .$$

The domain is discretized into 21 equally spaced particles with one particle at each end point, and h is set equal to 0.1. Figure 1a–c compares the kernel estimate of the function and of its first and the second derivatives as computed by the SPH, the CSPM and the MSPH methods with the exact solution. It is clear that the MSPH gives better results than the other two methods. Henceforth, we do not give results for the SPH method since the CSPM gives superior results than the SPH method.
The effect of increasing the number of particles from 21 to 51 is exhibited in Fig. 2a–c. As expected, the accuracy of the CSPM and the MSPH method is enhanced with the increase in the number of particles. However, the difference in the values of 2nd order derivatives computed by the CSPM and the exact solution is still large at particles near the boundaries. When third-order derivatives are retained in the expansion (3.1), the MSPH reproduces second-order derivatives of f at the end points but the CSPM does not; see Fig. 3a–c. For non-uniformly spaced 21 particles, Fig. 4a–c depicts a comparison of the kernel estimates of the function and its first two derivatives with their exact values. Particles are symmetrically located about $x = 0.5$ with $\Delta x_i = 1.2\Delta x_{i-1}$, $i = 11, 12, \ldots, 21$. The smoothing length h is set equal to $1.5\Delta x_i$. The errors in the kernel estimates of the first and the second derivatives near the end points of the domain are a little higher than those for the uniformly distributed particles. These errors can be reduced by increasing the number of particles.

3.4.2
Two-dimensional domain

For the function

$$f(x,y) = \sin \pi x \sin \pi y, \ x \in [0,1], \ y \in [0,1] \ ,$$

we have plotted in Fig. 5a–f the exact solution and the kernel estimates of the function and its first-order derivative, $f_{,x}$, computed with the CSPM and the MSPH method employing 21 equally spaced particles in each direction and $h = 0.1$. It is evident that the MSPH method yields a better estimate of the function f and of $f_{,x}$ than the CSPM. In each case, 2nd-order derivatives were retained in the expansion (3.1).

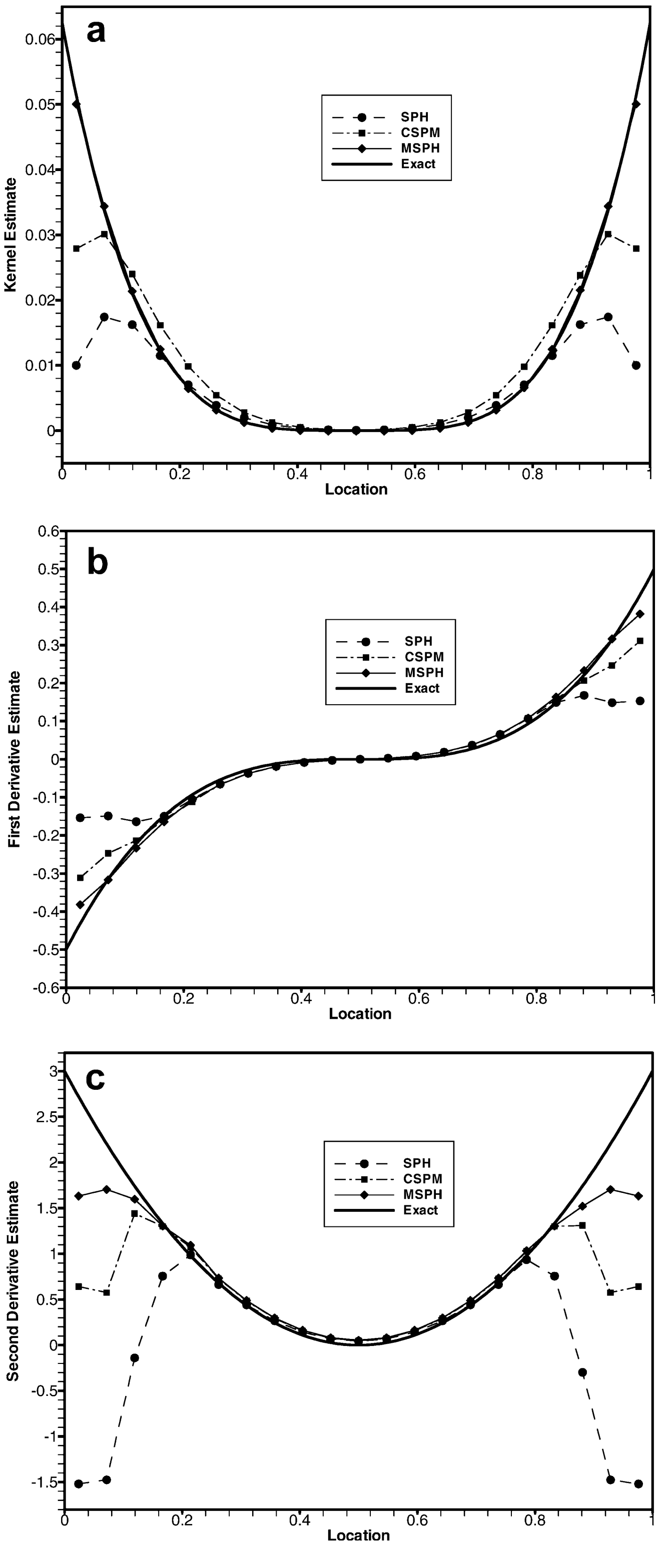

Fig. 1. Kernel estimates of **a** the function $(x-0.5)^4$, **b** its first derivative, and **c** its second derivative with 21 equally spaced particles on $[0,1]$

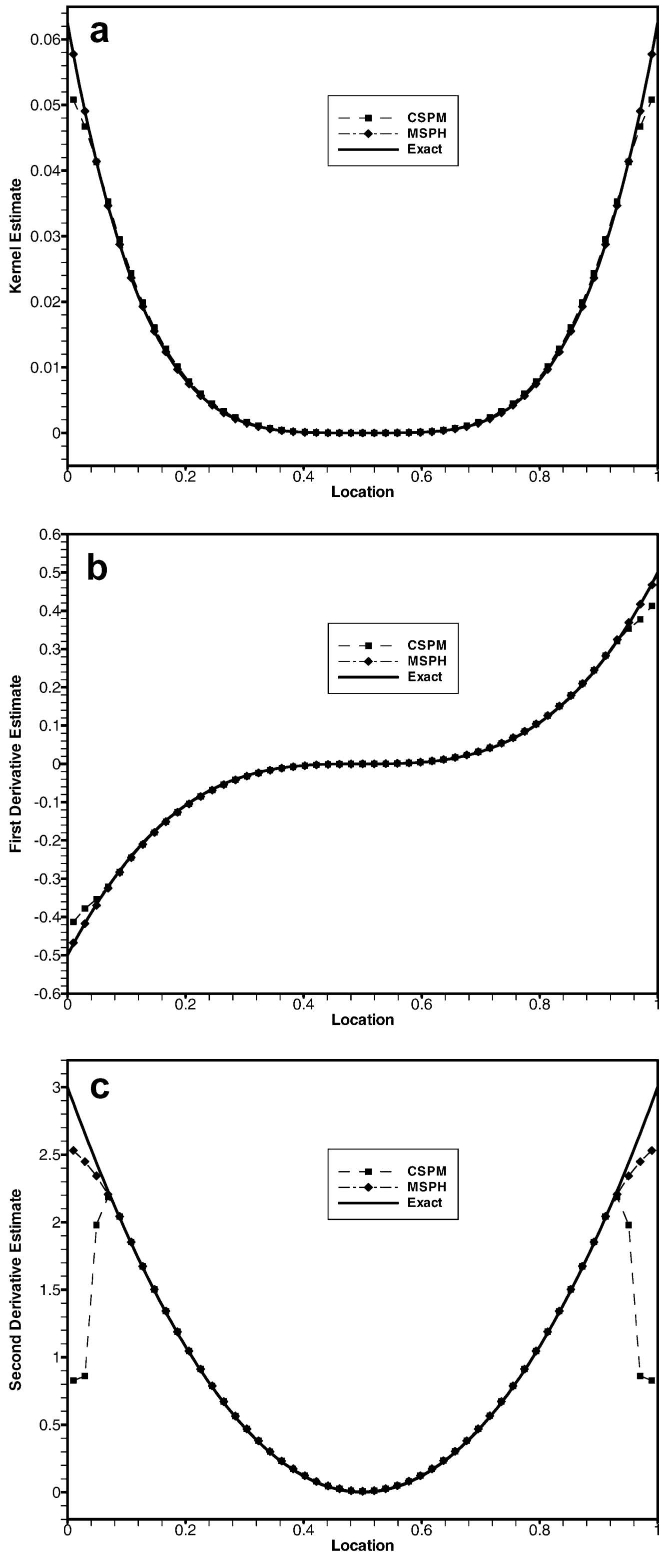

Fig. 2. Kernel estimates of **a** the function $(x-0.5)^4$, **b** its first derivative and **c** its second derivative with 51 equally spaced particles on $[0,1]$

4 Application of the MSPH to two transient problems

4.1 Wave propagation in an elastic bar

We use the MSPH method to study wave propagation in an elastic bar. The governing equations are

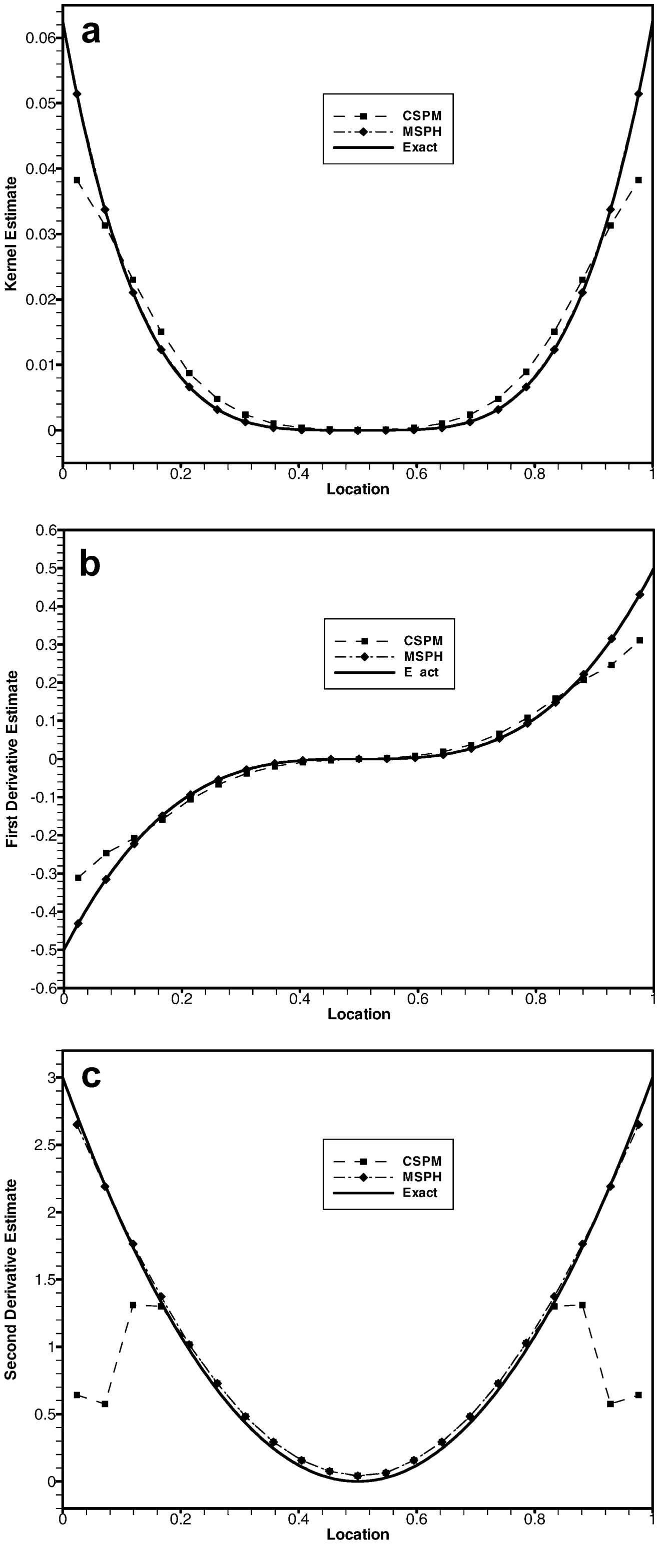

Fig. 3. Kernel estimates of **a** the function $(x - 0.5)^4$, **b** its first derivative, and **c** its second derivative with 51 equally spaced particles on $[0, 1]$ and the retention of 3rd-order derivatives in Eq. (3.1)

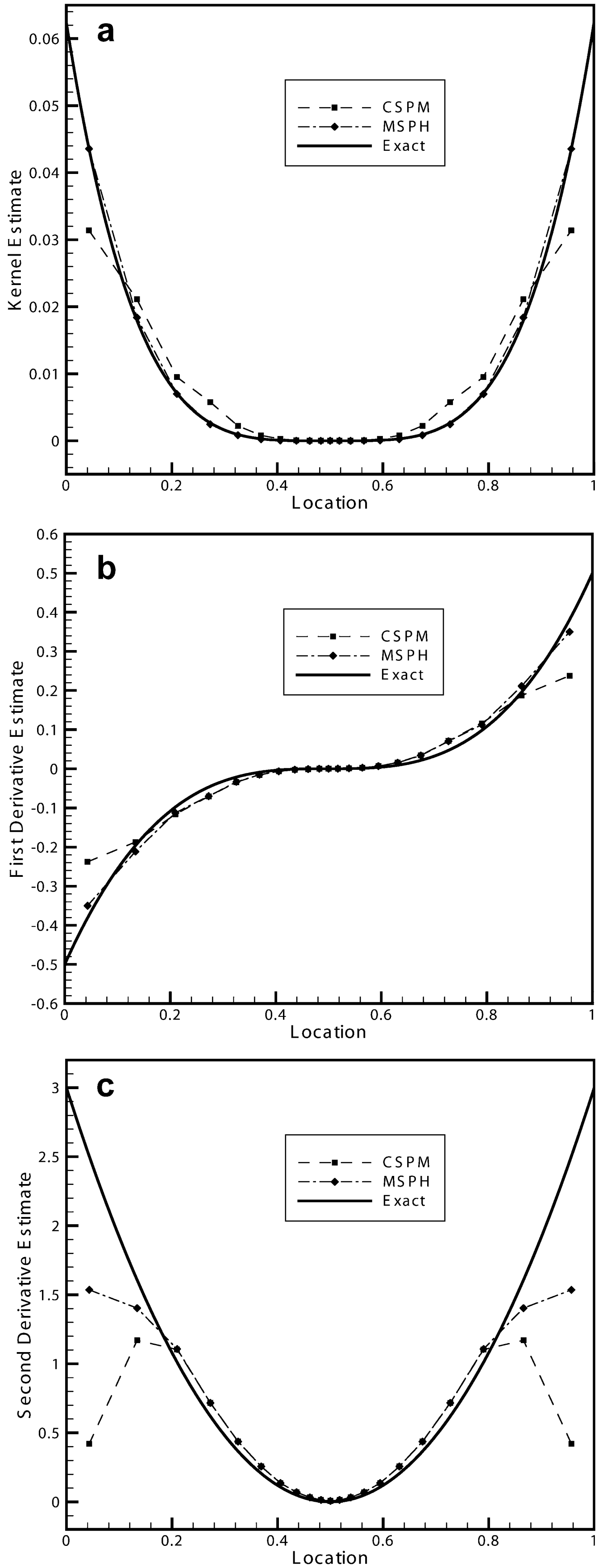

Fig. 4. Kernel estimates of **a** the function $(x - 0.5)^4$, **b** its first derivative, and **c** its second derivative computed with 21 irregularly spaced particles on [0,1]

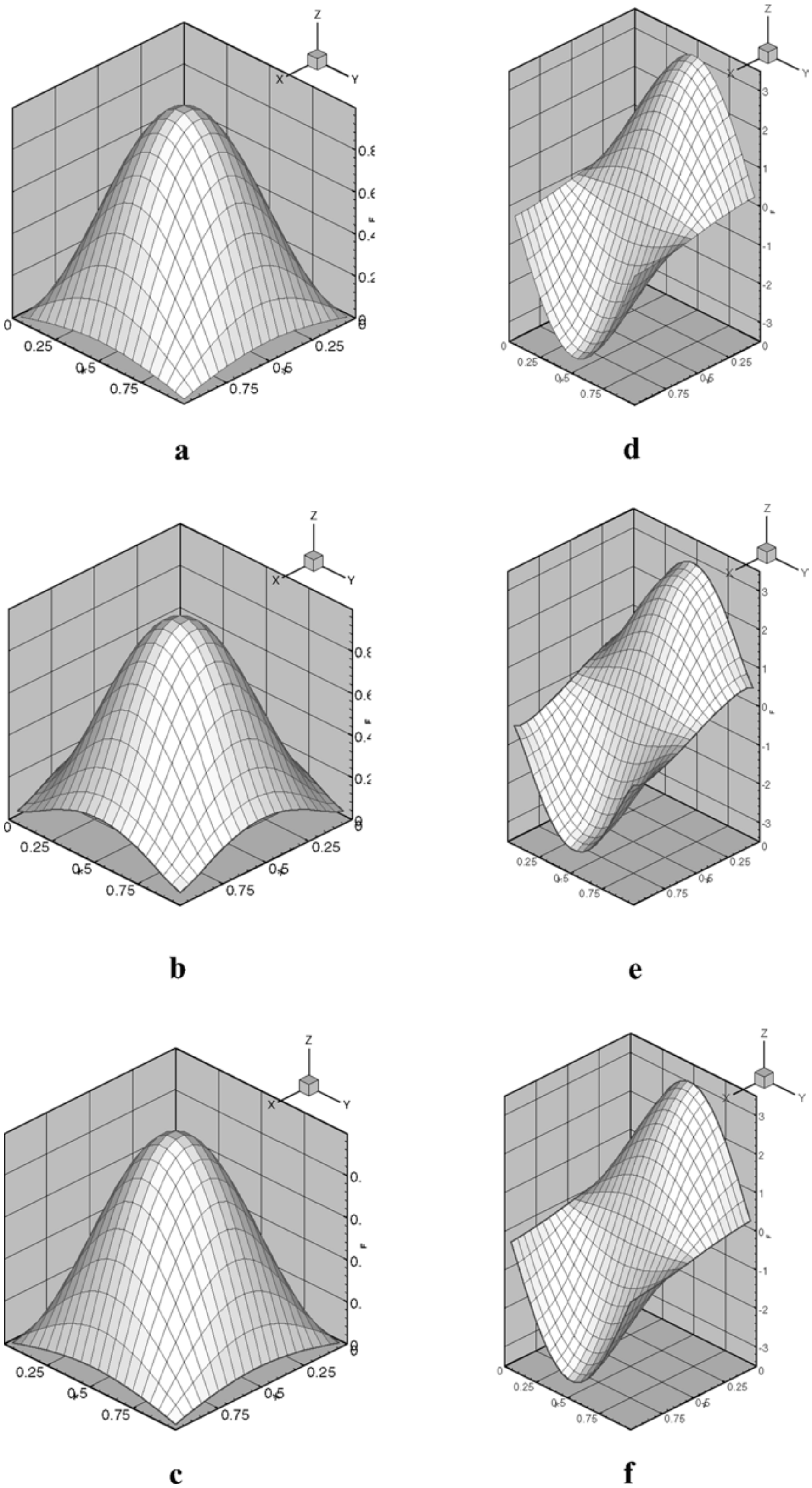

Fig. 5. **a** Plot of the function $f(x,y) = \sin \pi x \sin \pi y$, and kernel estimate of the function by **b** the CSPM, and **c** the MSPH methods; **d–f**: plot of $f_{,x}$–**d** exact solution, kernel estimate by **e** the CSPM,and **f** the MSPH methods

$$\dot{v} = \frac{1}{\rho}\sigma_{,x},$$
$$\dot{\sigma} = Ev_{,x},$$
$$\sigma(0,t) = 0,\ \sigma(0.1,t) = -[H(t-5\mu s) - H(t-0)]\text{GPa},$$
$$v(x,0) = 0,\ \sigma(x,0) = 0\ , \tag{4.1}$$

where v is the velocity of a material particle, σ the axial stress, $\sigma_{,x} = \partial\sigma/\partial x$, E Young's modulus, t time, and H the Heaviside step function. A rectangular compressive pulse of 5 μs duration and 1 GPa amplitude is applied at the end $x = 0.1$ m of the bar while the left end $x = 0$ of the bar is kept traction free. An artificial viscosity

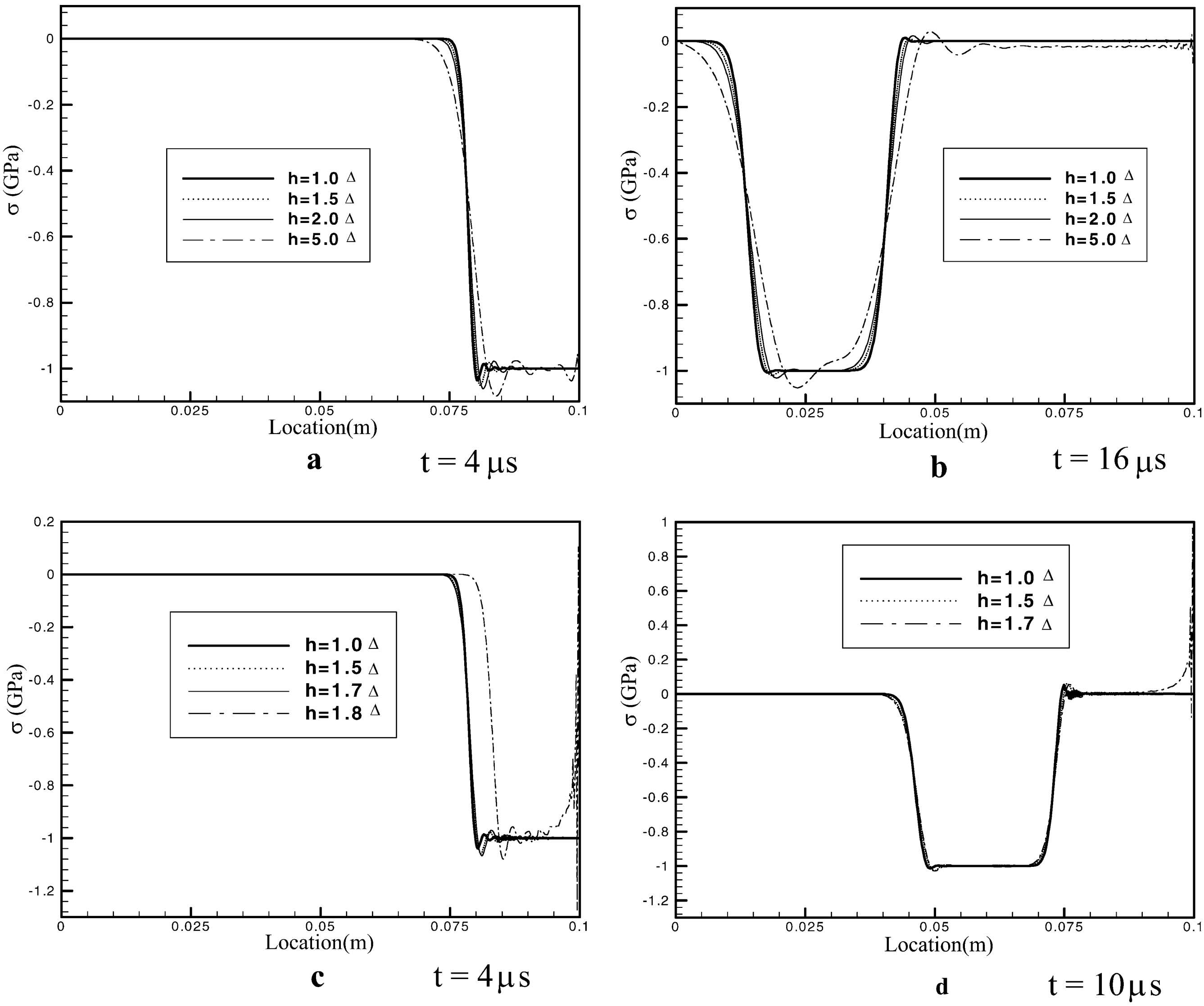

Fig. 6. Distribution of axial stress in the bar computed with $h = 1.0\Delta,\ 1.5\Delta,\ 2.0\Delta$ and 5.0Δ; **a**, **b** the MSPH method, **c**, **d** computed with the CSPM

is introduced in order to diminish oscillations. Accordingly, Eq. $(4.1)_1$ is modified to

$$\dot{v} = \frac{1}{\rho}(\sigma - \pi)_{,x} \ , \tag{4.2}$$

where

$$\pi = -0.2\rho c h v_{,x} + 4\rho h^2 (v_{,x})^2, \ \ v_{,x} < 0 \ , \tag{4.3}$$

where $c = \sqrt{E/\rho}$ is the wave speed.

Five hundred and one equally spaced particles are located on the 0.1 m long bar, and h is set equal to 0.3 mm or 1.5 times the distance, Δ, between two adjacent particles. In the MSPH method, the left-hand sides of eqns. $(4.2)_1$ and $(4.1)_2$ are evaluated at a particle and kernel estimates of $(\sigma - \pi)_{,x}$ and $v_{,x}$ are substituted on the right-hand sides. The value of $v_{,x}$ at time $(n - 1/2)$ is used to compute π. Recall that ρ and E are constants. The field variables in the MSPH equations are updated in time by using the leap-frog time integration scheme. That is,

$$v^{(n+1/2)} = v^{(n-1/2)} + \frac{1}{2}(\Delta t^n + \Delta t^{n-1})\dot{v}^n \ , \tag{4.4}$$

where $v^{n+1/2}$ is the value of v at time $t_{n+1/2}$, and $\Delta t^n = t_n - t_{n-1}$. The time step Δt is determined from

$$\Delta t = 0.3\Delta\sqrt{\frac{\rho}{E}} \ . \tag{4.5}$$

For $E = 227$ GPa and $\rho = 7800\ \mathrm{kg/m^3}$, $c = 5.393$ mm/μs is the speed of the elastic wave in the bar. It takes 18.5 μs for the wave to traverse the bar. The problem is analyzed by using the CSPM and the MSPH method. Figure 6a–d exhibits the distribution of the axial stress in the bar at $t = 4$ and 16 μs for the MSPH method, and at $t = 4$ μs and 10 μs for the CSPM. In both cases, results have been computed for $h = 1.0\Delta$, 1.5Δ, 2.0Δ and 5.0Δ. With $h = 1.0\Delta$ and $t = 30$ μs, the CPU time for the CSPM and the MSPH methods equalled 7.2 and 11.2 seconds respectively. Results plotted in Fig. 6 reveal that the amplitude of oscillations in

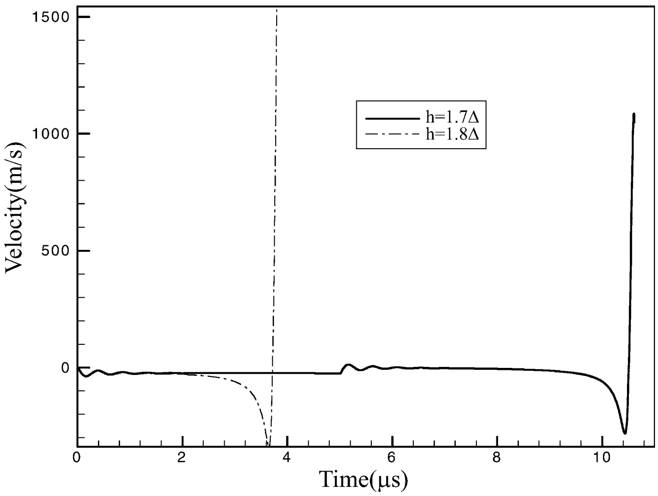

Fig. 7. Time history of the speed of the material particle at $x = 0.1$ m computed with the CSPM and $h = 1.7\Delta,\ 1.8\Delta$

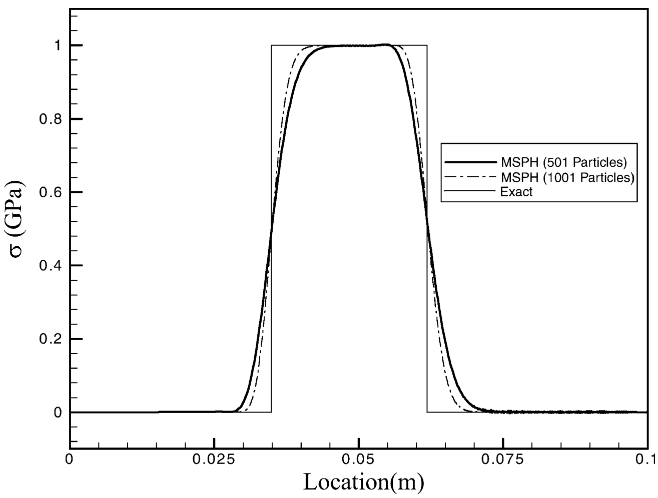

Fig. 8. Comparison of the axial stress distribution in the bar computed with the MSPH method using 501 and 1001 equally spaced particles with the analytical solution of the problem

the shock wave increases with an increase in the value of h. The speed of the shock wave computed with the two techniques is close to the analytical value of 5.395 mm/μs. For the CSPM and $h = 0.4$ mm, the solution exhibits oscillations at the right end $x = 0.1$ m where tractions are prescribed but no such oscillations are seen in the solution computed with the MSPH method. For the CSPM, the stress profile at the right end $x = 0.1$ m begins to become unstable at $t \simeq 3.2$ μs for $h = 1.8\Delta$ but the computation is stable at $t = 4$ μs for $h \leq 1.7\Delta$. For $h = 1.7\Delta$, the instability occurs at $t \simeq 10.0$ μs. The time history of the speed of the particle at $x = 0.1$ m computed with the CSPM and $h = 1.7\Delta$ and 1.8Δ is plotted in Fig. 7. We note that for $h = 1.5\Delta$, computations stay stable till $t = 30$ μs and possibly for longer times. However, the MSPH stays stable even when $h = 5\Delta$ as seen from the plots of Fig. 6a, b. Figure 8 compares stress distribution in the bar at $t = 30$ μs computed with the MSPH method and $\Delta = 0.2$ mm and 0.1 mm with the analytical solution of the problem. The compressive wave is reflected from the left free end as a tensile wave of amplitude 1 GPa.

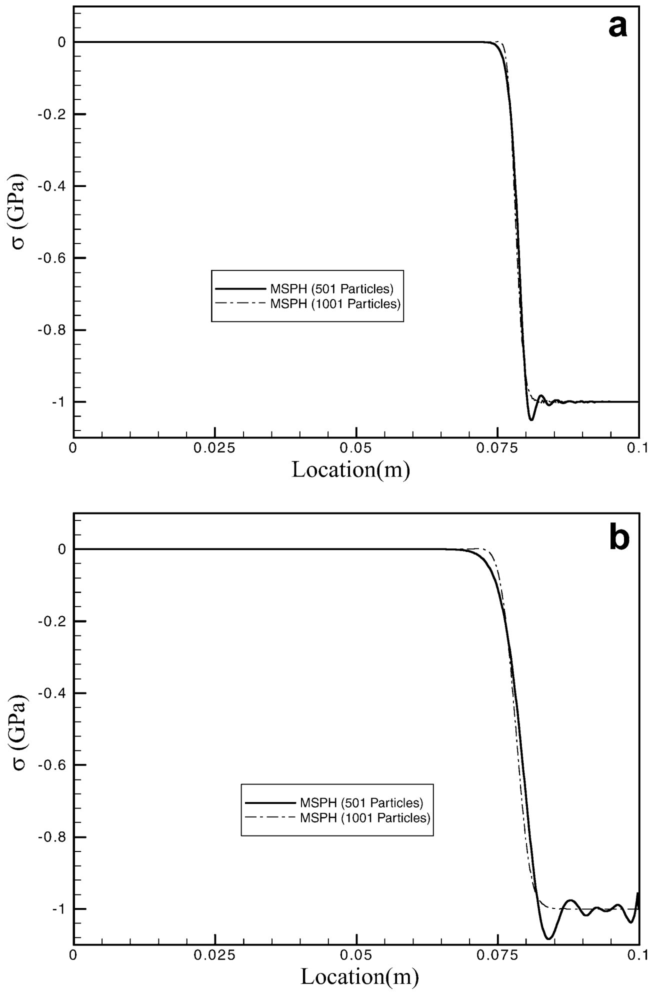

Fig. 9. Distribution of the axial stress in the bar at $t = 4$ μs computed with the MSPH method, and 501 and 1001 equally spaced particles; **a** $h = 1.5\Delta$, **b** $h = 5.0\Delta$

The rectangular shape of the wave is distorted because of numerical dissipation and the introduction of artificial viscosity. Results computed with 1001 equally spaced particles show improvement in the profile of the wave over that computed with 501 equally spaced particles. Figure 9 evinces that oscillations in the wave profile are diminished when third-order derivatives are retained in Eq. (3.1) and the solution computed with $h = 5\Delta$ is also quite smooth. We note that a larger value of h may be necessary in theories involving strain gradient as an independent variable, e.g. see Batra (1987) and Batra and Kim (1990).

4.2
Two-dimensional transient heat conduction

We use the MSPH method to solve

$$\frac{\partial T}{\partial t} = \frac{k}{\rho c}(T_{,xx} + T_{,yy}),\ (x,y) \in [0, 0.1\,m] \times [0, 0.1\,m]\ , \tag{4.6}$$

$$T(x,y,0) = 0\ , \tag{4.7}$$

$$T(0,y,t) = T(0.1,y,t) = T(x,0,t) = T(x,0.1,t) = 1\ . \tag{4.8}$$

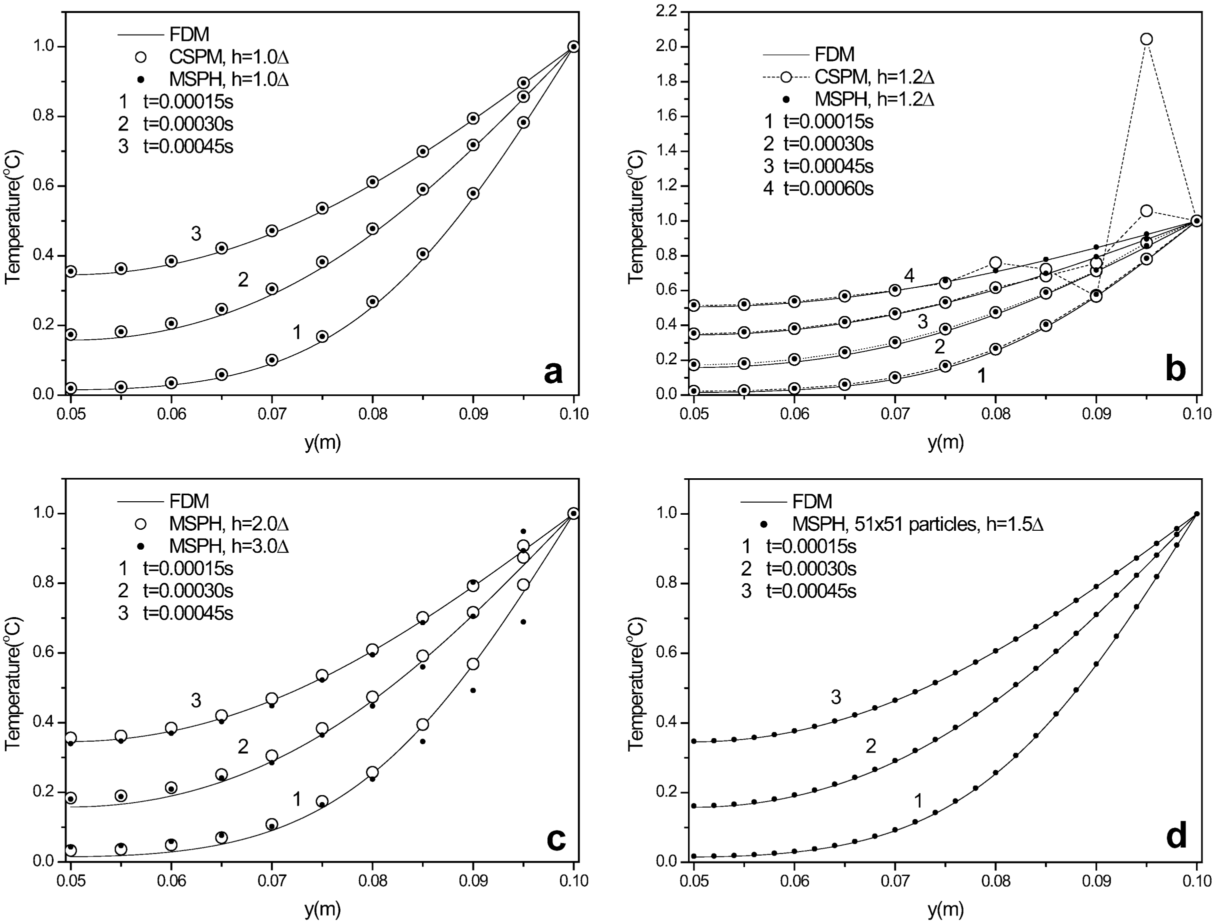

Fig. 10. Temperature distribution along the line $x = 0.05$ m; **a** 21×21 particles and $h = 1\Delta$, **b** 21×21 particles, $h = 1.2\Delta$, **c** 21×21 particles, $h = 2\Delta, 3\Delta$, **d** 51×51 particles, $h = 1.5\Delta$

Here T is the temperature, t the time, k the thermal conductivity, ρ the mass density, c the specific heat, and x and y are the spatial coordinates that vary between 0 and 0.1. The initial temperature of the plate is zero, and all edges are kept at a uniform temperature of 1 K. Because of the symmetry of the problem about the lines $x = 0.05$ m and $y = 0.05$ m, temperature distribution in the region $[0.05, 0.1] \times [0.05, 0.1]$ is computed with boundary conditions $T_{,x} = 0$ on $x = 0.05$ m and $T_{,y} = 0$ on $y = 0.05$ m. These boundary conditions are satisfied by including ghost particles in the region $x < 0.05$ m and $y < 0.05$ m. The temperature at a ghost particle is set equal to that of its mirror image about the lines $x = 0.05$ m and $y = 0.05$ m. Values of material parameters chosen are such that $k/(\rho c) = 1$.

The solution of the problem by the finite difference method (FDM) with 201×201 nodes is taken as the reference solution. For the CSPM and the MSPH method, 21×21 uniformly distributed particles and $h = 1.0\Delta$ are employed; Δ equals the distance between two neighboring particles. In each case (FDM, CSPM and the MSPH) the solution is marched forward in time by the conditionally stable forward-difference scheme. For the MSPH method, Eq. (4.6) is written at particle i and values of T_{xxi} and T_{yyi} are determined by solving linear simultaneous equations (3.5). The time increment employed is 1 μs. The temperature distribution along the line $x = 0.5$ m at three times, $t = 150,\ 300$ and 450 ms, computed with the three methods is depicted in Fig. 10a. The temperature found with the CSPM and the MSPH methods is a little higher than that with the FDM; this difference is due to the coarse distribution of particles. For $h = 1.2\Delta$, the CSPM solution exhibits oscillations near $y = 0.1$ m but the MSPH solution does not; cf. Fig. 10b. This may explain why $h = \Delta$ was used by Chen et al. (1999c). Figure 10c evinces MSPH results computed by taking $h = 2\Delta$ and 3Δ. The solution stays stable and agrees with that obtained by the FDM; the deviation between the two solutions can be diminished by employing more particles as shown in Fig. 10d where the MSPH solution computed with 51×51 uniformly spaced particles and $h = 1.5\Delta$ is exhibited. The temperature distribution computed with the MSPH method agrees well with the FDM solution.

In Fig. 11a–c, we present the locations of 21×21 unevenly spaced particles, and the spatial distribution of temperature on lines $x = 0.05$ m and $y = 0.05$ m. The distances between adjacent particles along the x-and y-axes are given by

$$\Delta x_I = \Delta x_{I-1}/1.05, \quad \Delta y_I = \Delta y_{I-1}/1.03 \ .$$

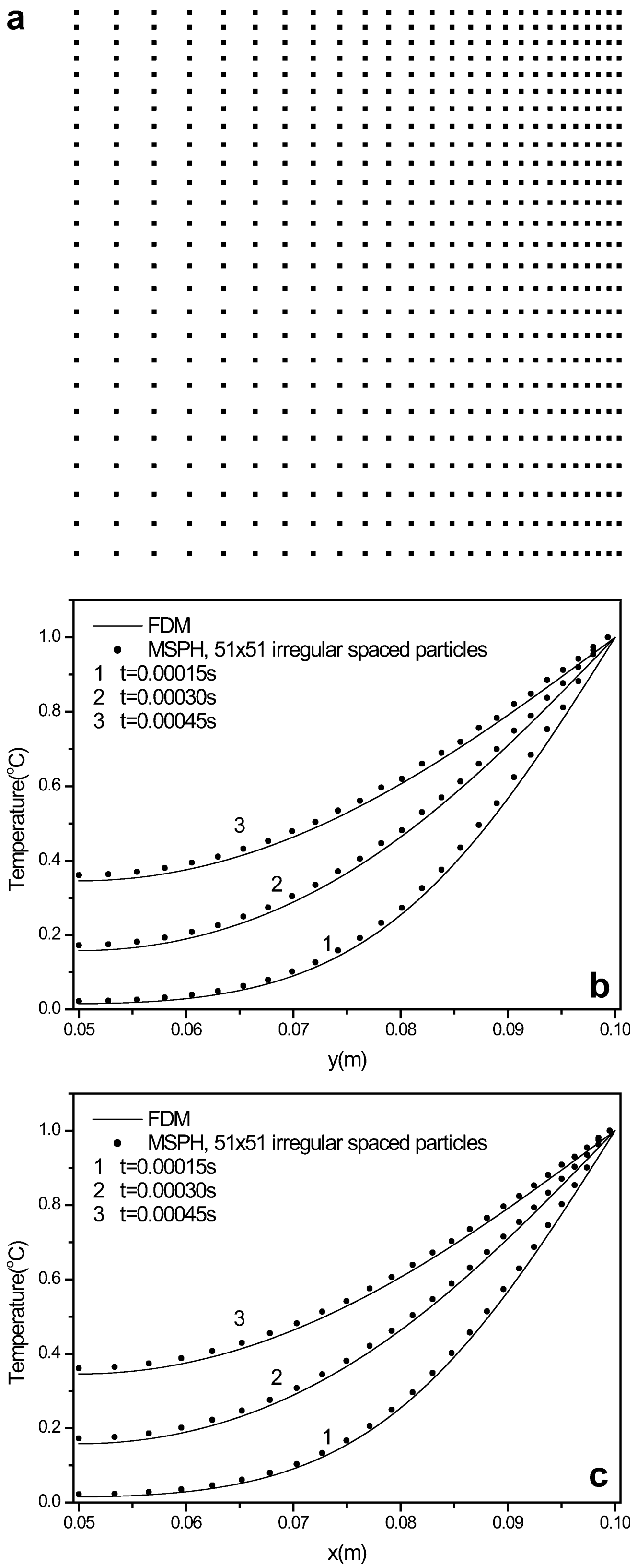

Fig. 11. **a** Distribution of irregularly spaced 21×21 particles in the North-East quarter of the plate, **b** and **c** Variation of temperature on lines $x = 0.05$ m and $y = 0.05$ m

Thus particles are closely packed near the boundaries $x = 0.1$ m and $y = 0.1$ m. The smoothing length h is taken to equal $1.5\max(\Delta x_I, \Delta y_I)$. Because of unequal values of Δx_I and Δy_I, different number of particles in the x- and the y-directions lie in the support of the kernel function. For the particle located at the top left corner, as many as four particles in the y-direction may lie in the support of its kernel. The temperature variations along the lines $x = 0.05$ m and $y = 0.05$ m plotted in Fig. 11b, c reveal that the nonuniform distribution of particles gives good results. The differences between the MSPH and the FDM results are a little higher for unequally spaced particles than those with equally spaced particles.

5
Conclusions

A modification to the CSPM method is proposed that improves the accuracy of the approximation at points near the boundaries of the domain. The superiority of the method has been established by approximating analytical functions defined on one- and two-dimensional domains. The method has been successfully applied to study wave propagation in an elastic bar and transient heat conduction in a plate.

References

Batra RC (1987) The initiation and growth of, and the interaction among, adiabatic shear bands in simple and dipolar materials. Int. J. Plasticity 3: 75–89

Batra RC, Kim CH (1990) Adiabatic shear banding in elastic-viscoplastic nonpolar and dipolar materials. Int. J. Plasticity 6: 127–141

Chen JK, Beraun JE, Jih CJ (1999a) An improvement for tensile instability in smoothed particle hydrodynamics. Comput. Mech. 23: 279–287

Chen JK, Beraun JE, Jih CJ (1999b) Completeness of corrective smoothed particle method for linear elastodynamics. Comput. Mech. 24: 273–285

Chen JK, Beraun JE, Carney TC (1999c) A corrective smoothed particle method for boundary value problems in heat conduction. Int. J. Numer. Meth. Eng. 46: 231–252

Gingold RA, Monaghan JJ (1977) Smoothed particle hydrodynamics: Theory and application to non-spherical stars. Mon. Not. Roy Astron. Soc. 181: 375–389

Johnson GR, Stryk RA, Beissel SR (1996) SPH for high velocity impact computations. Comput. Meth. Appl. Mech. Engrg. 139: 347–373

Libersky LD, Petschek AG (1990) Smooth particle hydrodynamics with strength of materials, advances in the free Lagrange method. Lecture Notes in Physics 395: 248–257

Liu MB, Liu GR, Zhong Z, Lam KY (2003) Computer simulation of high explosive explosion using smoothed particle hydrodynamics methodology. Comput. Fluids 32(3): 305–322

Liu WK, Jun S, Li S, Adee J, Belytschko T (1995a) Reproducing Kernel Particle Methods for structural dynamics. Int. J. Numer. Methods Eng. 38: 1655–1679

Liu WK, Jun S, Zhang YF (1995b) Reproducing Kernel Particle Methods. Int. J. Numer. Methods Fluids 20: 1081–1106

Lucy LB (1977) A numerical approach to the testing of the fission hypothesis. Astron. J. 82: 1013–1024

Medina DF, Chen JK (2000) Three-dimensional simulations of impact induced damage in composite structures using the parallelized SPH method. Composites Part A 31: 853–860

Monaghan JJ (1994) Simulating free surface flows with SPH. J. Comput. Phys. 110: 399–406

Randles PW, Carney TC, Libersky LD, Renick JD, Petschek AG (1995) Calculation of oblique impact and fracture of tungsten cubes using smoothed particle hydrodynamics. Int. J. Impact Eng. 17: 661–672